Journal of
Applied Physics

Electric-field control of electronic transport properties and enhanced magnetoresistance in $La_{0.7}Sr_{0.3}MnO_3$/0.5$BaZr_{0.2}Ti_{0.8}O_3$-0.5$Ba_{0.7}Ca_{0.3}$ lead-free multiferroic structures

Cite as: J. Appl. Phys. **122**, 134102 (2017); https://doi.org/10.1063/1.4990513
Submitted: 15 June 2017 . Accepted: 17 September 2017 . Published Online: 02 October 2017

Jian-Min Yan, Guan-Yin Gao, Yu-Kuai Liu, Fei-Fei Wang, and Ren-Kui Zheng

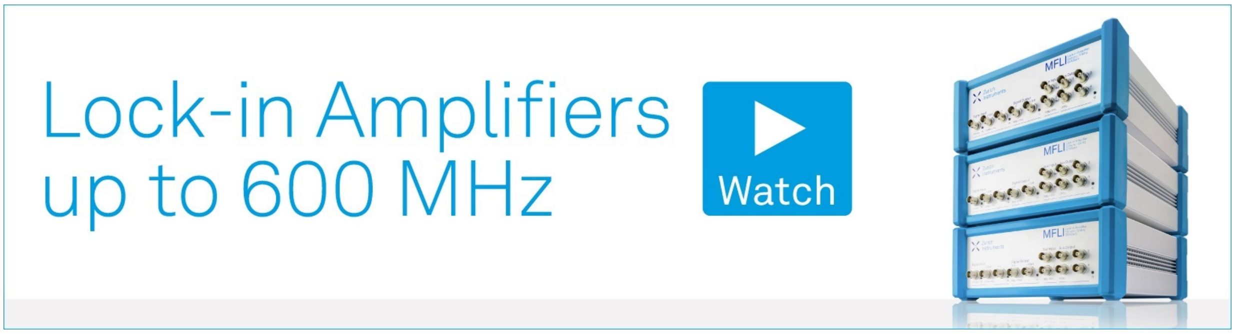

J. Appl. Phys. **122**, 134102 (2017); https://doi.org/10.1063/1.4990513 **122**, 134102

JOURNAL OF APPLIED PHYSICS **122**, 134102 (2017)

Electric-field control of electronic transport properties and enhanced magnetoresistance in $La_{0.7}Sr_{0.3}MnO_3$/$0.5BaZr_{0.2}Ti_{0.8}O_3$-$0.5Ba_{0.7}Ca_{0.3}TiO_3$ lead-free multiferroic structures

Jian-Min Yan,[1,2] Guan-Yin Gao,[3] Yu-Kuai Liu,[4,a)] Fei-Fei Wang,[1,a)] and Ren-Kui Zheng[2,a)]
[1]*Key Laboratory of Optoelectronic Material and Device, Department of Physics, Shanghai Normal University, Shanghai 200234, China*
[2]*State Key Laboratory of High Performance Ceramics and Superfine Microstructure, Shanghai Institute of Ceramics, Chinese Academy of Sciences, Shanghai 200050, China*
[3]*Hefei National Laboratory for Physical Sciences at Microscale, University of Science and Technology of China, Hefei 230026, China*
[4]*Department of Applied Physics, The Hong Kong Polytechnic University, Hong Kong, China*

(Received 15 June 2017; accepted 17 September 2017; published online 2 October 2017)

We report the fabrication of lead-free multiferroic structures by depositing ferromagnetic $La_{0.7}Sr_{0.3}MnO_3$ (LSMO) polycrystalline films on polished $0.5BaZr_{0.2}Ti_{0.8}O_3$-$0.5Ba_{0.7}Ca_{0.3}TiO_3$ (BZT-BCT) piezoelectric ceramic substrates. By applying electric fields to the BZT-BCT along the thickness direction, the resistivity of LSMO films can be effectively manipulated *via* the piezoelectric strain of the BZT-BCT. Moreover, the LSMO polycrystalline films exhibit almost temperature independent and significantly enhanced magnetoresistance (MR) below T_C. At $T = 2$ K and $H = 8$ T, the MR of polycrystalline films is approximately two orders of magnitude higher than that of LSMO epitaxial films grown on $(LaAlO_3)_{0.3}(SrAl_{1/2}Ta_{1/2}O_3)_{0.7}$ single-crystal substrates. The enhanced MR mainly results from the spin-polarized tunneling of charge carriers across grain boundaries. The LSMO/BZT-BCT structures with electric-field controllable modulation of resistivity and enhanced MR effect may have potential applications in low-energy consumption and environmentally friendly electronic devices. *Published by AIP Publishing.*
https://doi.org/10.1063/1.4990513

I. INTRODUCTION

Layered artificial multiferroic heterostructures employing ferromagnetic (FM) and ferroelectric (FE) materials have attracted much attention in the past decade because of their strong room-temperature magnetoelectric (ME) coupling effects and great flexibility in material selection and device design.[1–4] One of the most facile and promising approaches to construct FM/FE layer structures is to directly grow FM films on FE substrates. Until now, lead-based piezoelectric single crystals and ceramics are usually used as substrates to grow FM films since they show excellent piezoelectric and ferroelectric properties. Such FM/FE layered structures include perovskite manganite film/$Pb(Mg_{1/3}Nb_{2/3})O_3$-$PbTiO_3$ (PMN-PT),[4–6] ferrite film/PMN-PT,[7,8] FM alloy film/PMN-PT,[9,10] Fe_3O_4/PZT,[11] FeGe/PZT,[12] etc. One of the key concerns in these multiferroic structures is that the FE layers contain a large amount of environmentally unfriendly lead element (approximately 68 wt. % in terms of PbO). Although FM films have been successfully grown on several lead-free multiferroic single-crystal substrates to form FM/FE multiferroic structures including the $Co_{40}Fe_{40}B_{20}$/$YMnO_3$,[13] it is rather difficult to modulate the electrical and magnetic properties of the $Co_{40}Fe_{40}B_{20}$ films by applying electric fields to the $YMnO_3$ substrates which show very weak ferroelectricity and piezoelectricity. Therefore, it is highly desirable to fabricate lead-free FM/FE multiferroic structures with strong magnetoelectric coupling effects at room temperature and study their physical properties. Unfortunately, there have been few studies focusing on lead-free FM film/FE substrate structures until now.

$BaTiO_3$ is a prototypical lead-free piezoelectric material that has been used in capacitors, electromechanical transducers, and nonlinear optics. However, there are very limited reports on $BaTiO_3$ single crystal- or ceramics-based FM/FE structures,[14–20] which may probably due to the relatively low piezoelectric coefficient of $BaTiO_3$ ($d_{33}\sim190$ pC/N) and the high probability of failure or crack of crystals when they are repeatedly driven by external electric fields. Recently, Liu and Ren[21] reported that lead-free $0.5BaZr_{0.2}Ti_{0.8}O_3$-$0.5Ba_{0.7}Ca_{0.3}TiO_3$ (BZT-BCT) piezoelectric ceramics exhibit a large $d_{33}\sim620$ pC/N which is comparable to that of PZT ceramics. Moreover, BZT-BCT ceramics have perovskite structures with lattice parameters $a\sim b\sim c\sim4.0$ Å that are very close to those of PMN-PT ($a\sim b\sim c\sim4.02$ Å) and PZT ($a\sim b\sim c\sim4.03$ Å). Therefore, BZT-BCT is a good candidate material for the fabrication of lead-free multiferroic structures. Among a variety of FM materials, $La_{0.7}Sr_{0.3}MnO_3$ (LSMO) is a half metallic compound with ferromagnetic Curie temperature ($T_C\sim370$ K) far above room temperature and exhibits a range of attractive physical phenomena such as the colossal magnetoresistance (MR) effect and electronic phase separation. Furthermore, the electronic and magnetic properties of LSMO films are sensitive to lattice strains because of the strong interplay among the spin, charge, and lattice degrees of freedom.[4–6,22]

[a)] Authors to whom correspondence should be addressed. ffwang@shnu.edu.cn; liuyk@mail.ustc.edu.cn; and zrk@ustc.edu

In this article, we report the fabrication of LSMO/BZT-BCT layered FM/FE structures by growing LSMO polycrystalline films with different thicknesses on polished BZT-BCT ceramic substrates. The resistivity of LSMO films can be tuned and modulated by the electric-field-induced reversible piezoelectric strain in the BZT-BCT layer. Magnetotransport measurements demonstrate that the LSMO polycrystalline films show significantly enhanced and almost temperature independent magnetoresistance (MR) from 10 to 275 K (close to T_C of the LSMO polycrystalline film), which is explained in terms of spin polarized tunneling of charge carriers across grain boundaries.

II. EXPERIMENTAL

BZT-BCT ceramics were synthesized by the solid state reaction method. The starting materials of $BaCO_3$(99.8%), $CaCO_3$(99.5%), ZrO_2(99.99%), and TiO_2(99.9%) were weighed in a stoichiometric amount and ball milled in ethanol for 24 h. The mixtures were calcinated at 1300 °C for 2 h and ball milled again in ethanol for 24 h. Then, the powders were pressed into 10 mm diameter pellets which were sintered at 1540 °C for 4 h, followed by cooling to room temperature at 5 °C/min. The relative density of the sintered ceramics is approximately 98.3%. Finally, one-side surface of each BZT-BCT ceramic was carefully polished to an average roughness of ∼5 nm and a thickness of ∼0.5 mm. LSMO films were grown on such polished ceramic substrates and $(LaAlO_3)_{0.3}(SrAl_{1/2}Ta_{1/2}O_3)_{0.7}$ (LSAT) single-crystal substrates by the pulsed laser deposition using a KrF excimer laser (λ = 248 nm). Film deposition was carried out at a substrate temperature of 700 °C and an oxygen pressure of 27 Pa. The laser energy density and repetition rate were 3 J/cm^2 and 5 Hz, respectively. After deposition, the LSMO films were *in situ* annealed in 1 atm oxygen atmosphere for 1 h to reduce oxygen deficiencies. The thickness of LSMO films is controlled by the number of laser pulses.

The crystallographic properties and phase purity of LSMO films were examined by x-ray diffraction (XRD) θ-2θ scans using a Bruker D8 Advance x-ray diffractometer with Cu $K_{\alpha 1}$ radiation ($\lambda = 1.5406$ Å). The surface morphology and roughness of polished BZT-BCT ceramic substrates were checked through atomic force microscopy (AFM) images that were obtained using a Dimension V (Veeco) scanning probe microscope. The resistivity of LSMO films was measured using a physical property measurement system (PPMS-9, Quantum Design). Ferroelectric hysteresis loops and piezoelectric coefficients of BZT-BCT substrates were measured using a Precision Multiferroic Analyzer (Radiant Technologies, Inc. USA) and a d_{33}-meter (ZJ-3A, China), respectively.

III. RESULTS AND DISCUSSION

Figure 1(a) shows the surface morphology of a polished BZT-BCT ceramic substrate which shows a root mean square roughness of ∼5 nm. The room-temperature ferroelectric hysteresis loop of the BZT-BCT substrate is shown in Fig. 1(b), where the remnant polarization $2P_r$ is ∼24 μC/cm^2. The piezoelectric coefficient d_{33} of the BZT-BCT substrate reaches a high value of ∼615 pC/N, which is close to that (620 pC/N) reported by Liu and Ren.[21] The fairly good piezoelectric and ferroelectric properties, together with the relatively smooth surface, make the polished BZT-BCT ceramics suitable substrates to grow LSMO films. Figure 1(c) displays the XRD patterns of LSMO films with different thicknesses grown on BZT-BCT substrates. The patterns were measured using the schematic experimental setup shown in Fig. S1(a) (supplementary material). Nine diffraction peaks from the BZT-BCT substrates appear, indicating the polycrystalline nature of the ceramic substrates. Besides these peaks, the LSMO (104) peaks can be seen at 2θ=32.62° for the LSMO film with a thickness of ∼64 nm. Note that this peak is the strongest diffraction peak of LSMO polycrystalline samples with a rhombohedral symmetry, indicating that the LSMO film is polycrystalline. Because of this reason, the LSMO (104) and

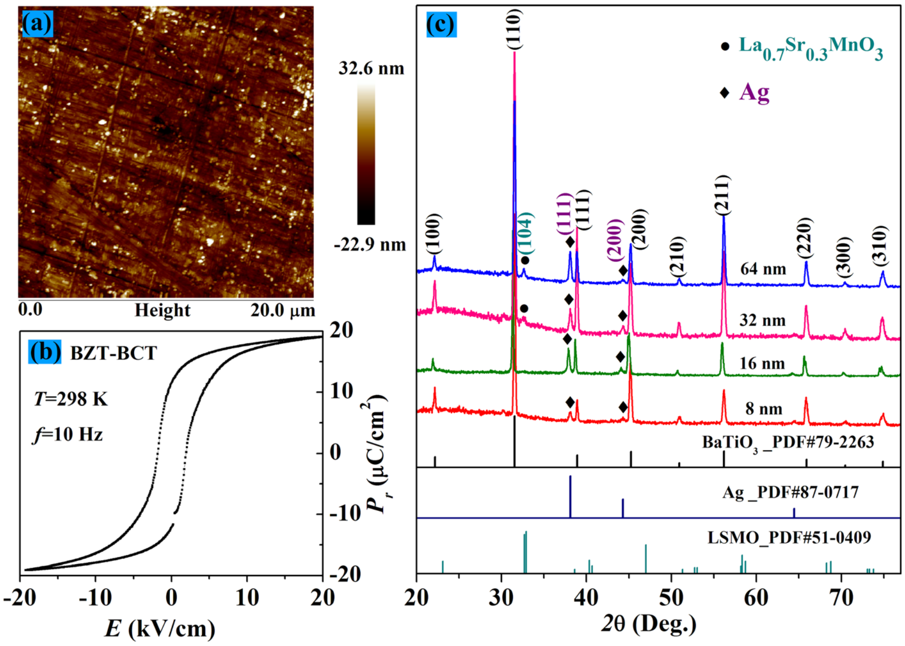

FIG. 1. (a) Surface morphology of a polished BZT-BCT ceramic substrate as measured using an atomic force microscope. (b) Ferroelectric hysteresis loop of a BZT-BCT substrate as measured at $T = 298$ K. (c) X-ray diffraction patterns of LSMO/BZT-BCT structures with different film thicknesses.

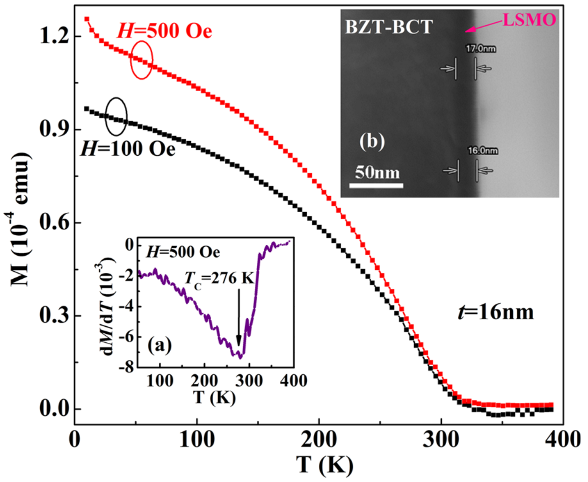

FIG. 2. Temperature dependence of the field-cooled magnetization as a function of temperature for the LSMO film (~16 nm) grown on the BZT-BCT substrate. Insets: (a) The d*M*/d*T* *versus* *T* for the LSMO film, (b) a cross-sectional SEM image of a LSMO/BZT-BCT structure with a film thickness of ~16 nm.

other diffraction peaks for thinner LSMO films ($t = 8$, 16, 32 nm) cannot be detected by XRD. Magnetization measurements on LSMO/BZT-BCT structures with film thicknesses of ~16, 32, 64, and 128 nm demonstrate that the LSMO polycrystalline films grown on the BZT-BCT substrates exhibit ferromagnetic behaviors below room temperature [Figs. 2 and S2 (supplementary material)].

Previous studies demonstrated that, for layered perovskite manganite film/FE single-crystal substrate (FE = PMN-PT, $BaTiO_3$) multiferroic structures, the electric-field-induced lattice strain in FE substrates plays a dominant role in the modulation of ferromagnetism and resistivity of manganite films while the electric-field-induced polarization charges at the interface have minor effects on the properties of manganite films.[4–6,14–20,22] To clarify which effect is more important in the present LSMO/BZT-BCT structures, we measured the relative resistivity changes ($\Delta\rho/\rho$) of the 16 nm LSMO film at different fixed temperatures by applying bipolar electric fields (E) to the BZT-BCT substrate along the thickness direction, using the schematic experimental setup shown in Fig. S1(b) (supplementary material), and showed the results in Fig. 3. Note that the $\Delta\rho/\rho$ *versus* E curves for LSMO films with other thicknesses (~8, 32, and 64 nm) are shown in Figs. S3–S5 (supplementary material). Here, $\Delta\rho/\rho = [\rho(E) - \rho(0)]/\rho(0)$, where $\rho(E)$ and $\rho(0)$ are the resistivity of LSMO films in the presence and absence of electric fields, respectively. It can be seen that the $\Delta\rho/\rho$ *versus* E curve at $T = 300\,K$ exhibits a fairly well butterfly-like shape, which is similar to that of the electric-field-induced in-plane strain (ε_{xx}) *versus* E curve at $T = 300\,K$ (Fig. S6, supplementary material). It is thus established that the resistivity changes are caused by the electric-field-induced piezoelectric strain in the BZT-BCT substrate. The $\Delta\rho/\rho$ *versus* E curves obtained at higher temperatures (e.g., 315, 330, and 345 K) also show a butterfly-like shape [Figs. 3(a)–3(c)], implying a similar underlying mechanism as that at $T = 300\,K$. However, with decreasing temperature from 300 K the butterfly-like shape of the $\Delta\rho/\rho$ *versus* E curve becomes asymmetric at $T = 285$, 270, 240, 210, and 180 K, and completely disappears at $T = 150\,K$, where the $\Delta\rho/\rho$ *versus* E curve exhibits a rectangle-like shape. With further decrease in the temperature, the $\Delta\rho/\rho$ *versus* E curve shows a shrunken rectangle shape at $T = 90\,K$. To clarify the origin of the asymmetric butterfly-like curves at low temperatures, the electric-field-induced in-plane strain (ε_{xx}) of a BZT-BCT substrate was measured as a function of bipolar E at several low temperatures. The ε_{xx} *versus* E curves also show an asymmetric butterfly-like shape at $T = 240$ and

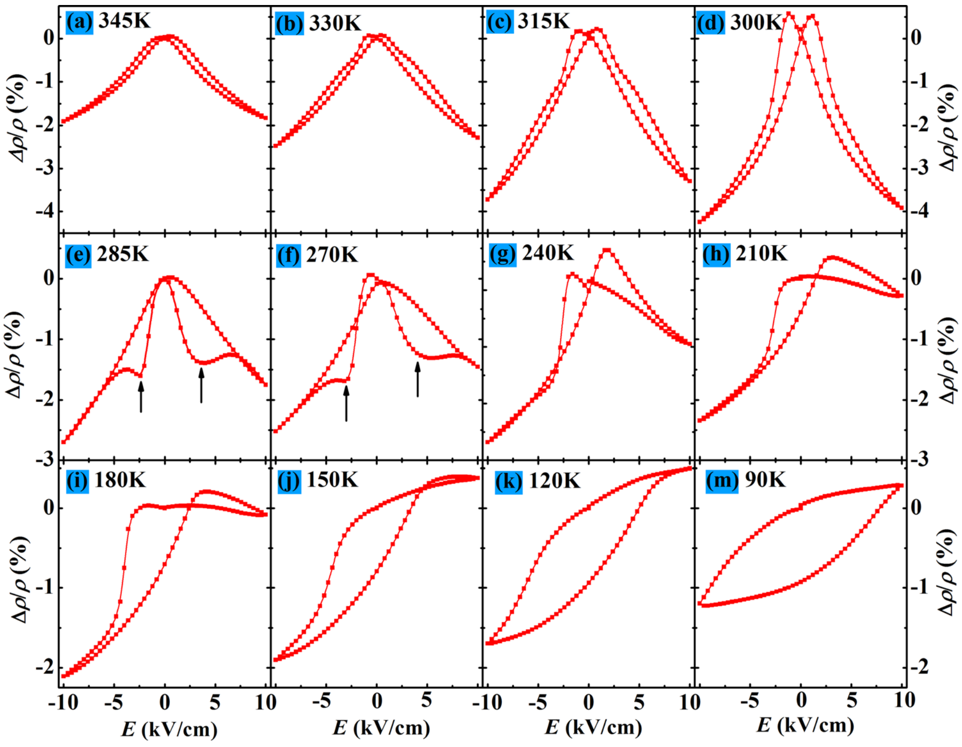

FIG. 3. [(a)–(m)] Relative resistivity changes ($\Delta\rho/\rho$) of the LSMO film (~16 nm) at various fixed temperatures as a function of bipolar electric field applied to the BZT-BCT substrate.

210 K (Fig. S6, supplementary material), which is similar to the shapes of the $\Delta\rho/\rho$ *versus* E curves at low temperatures, thus demonstrating the piezoelectric strain-driven nature of the resistivity changes at low temperatures. With decreasing temperature from room temperature, the BZT-BCT evolves from the two-phase (i.e., the tetragonal and rhombohedral) coexistence region to the one-phase (i.e., the rhombohedral) region,[21] which would suppress the piezoelectricity of the BZT-BCT. Moreover, with decreasing temperature ferroelectric domains would be frozen to some degree, which would result in a reduction of the piezoelectricity. Consequently, the piezoelectric strain effect is suppressed with decreasing temperatures, which is reflected by the decrease in $\Delta\rho/\rho$ with decreasing temperature (Fig. S7, supplementary material). Another noteworthy feature is the abnormal concave downward in the $\Delta\rho/\rho$ *versus* E curves at $T = 285$ and 270 K near $E \sim \pm 2.5$ kV/cm [Figs. 3(e) and 3(f)]. Both the dielectric constant *versus* temperature curves for the BZT-BCT substrate (see Fig. S8, supplementary material) and the recently reported phase diagram of BZT-BCT[23] show that the rhombohedral and orthorhombic phases coexist in the BZT-BCT ceramics near $T \sim 280$ K. Therefore, the anomalies in $\Delta\rho/\rho$ near $E \sim \pm 2.5$ kV/cm is very possibly due to the electric-field-induced rhombohedral-to-orthorhombic phase transformation which would induce the lattice strain.[24]

To probe into the MR effect in the LSMO polycrystalline films grown on the BZT-BCT substrates, we measured the resistivity of the 16 nm LSMO film from 2 to 380 K in magnetic fields up to $H = 9$ T. For comparison purpose, we also measured the resistivity of a LSMO epitaxial film with a similar thickness grown on a (001)-oriented LSAT single-crystal substrate. The XRD θ-2θ and ϕ-scan patterns (Fig. S9, supplementary material) confirm the good epitaxy of the LSMO film on the LSAT substrate. Figures 4(a) and 4(c) show the temperature dependence of the resistivity for the LSMO films ($\sim$16 nm) grown on the BZT-BCT and LSAT substrates, respectively. The metal-to-insulator transition temperature (T_{MI}) of the LSMO polycrystalline film ($\sim$325 K) is lower than that of the LSMO epitaxial film whose T_{MI} ($\sim$380 K) is close to that ($\sim$378 K) of the LSMO single crystals. Moreover, the resistivity of the LSMO polycrystalline film at any fixed temperature is higher than that of the epitaxial one. Due to the existence of a large number of grain boundaries in polycrystalline films, the electronic transport properties of LSMO films would be greatly influenced by the grain boundaries which act as electron transport barriers.[25,26] In contrast, high-quality epitaxial films have much less grain boundaries,[27] resulting in reduced effects of grain boundaries.

Figures 4(b) and 4(d) show the temperature dependence of MR for the 16 nm LSMO films grown on the BZT-BCT and LSAT substrates, respectively. Here, $\mathrm{MR} = [\rho(0) - \rho(\mathrm{H})]/\rho(0)]$, where $\rho(0)$ and $\rho(\mathrm{H})$ are the resistivity of the LSMO films in the absence and presence of magnetic fields, respectively. For the LSMO epitaxial film, the MR shows the maximum near the paramagnetic-to-ferromagnetic phase transition temperature $\mathrm{T_C}$ and decreases sharply when the temperature deviates from $\mathrm{T_C}$. Moreover, the MR effects of the epitaxial film in the ferromagnetic ground state (e.g., $\mathrm{T} = 2$ K) are very weak ($\mathrm{MR} = 0.4\%$ at $\mathrm{H} = 8$ T). These magnetotransport properties of the LSMO epitaxial film are similar to those of LSMO single crystals, reflecting the intrinsic magnetoresistance effect of the LSMO epitaxial film. These overall magnetotransport behaviors of the LSMO epitaxial film could be understood within the framework of the double-exchange interaction, electron-lattice coupling, and the electronic phase separation.[28,29]

For the LSMO polycrystalline film, the magnetoresistance effects in the ferromagnetic ground state (e.g., $T = 2$ K)

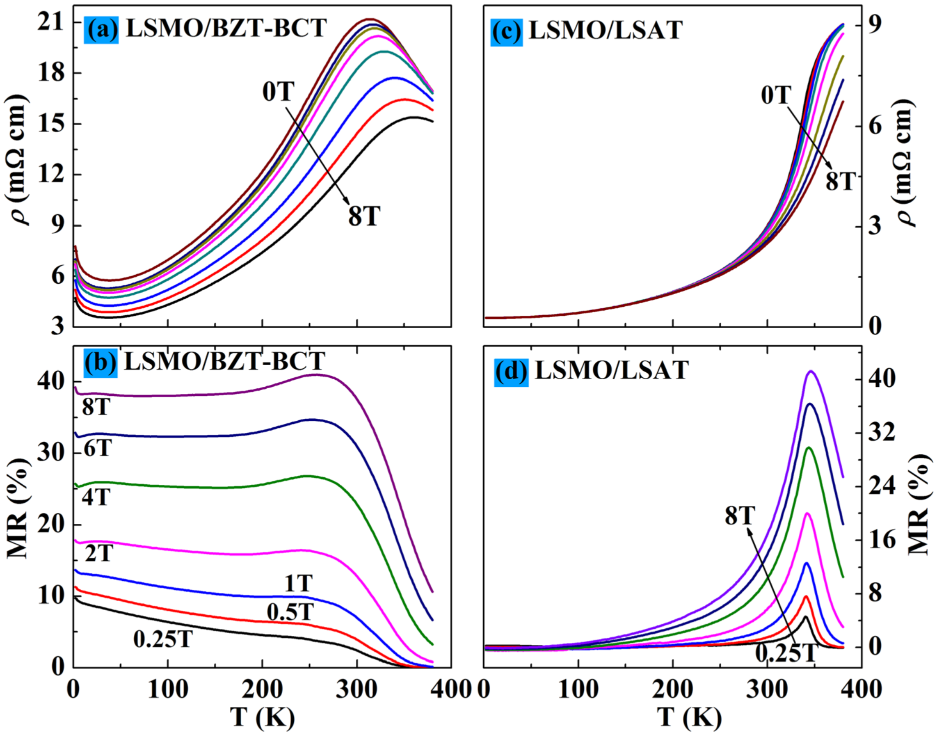

FIG. 4. Temperature dependence of the resistivity for the LSMO films ($\sim$16 nm) grown on (a) BZT-BCT and (c) LSAT substrates in different magnetic fields. (b) and (d) show the magnetoresistance as a function of temperature for the LSMO films ($\sim$16 nm) grown on BZT-BCT and LSAT substrates, respectively.

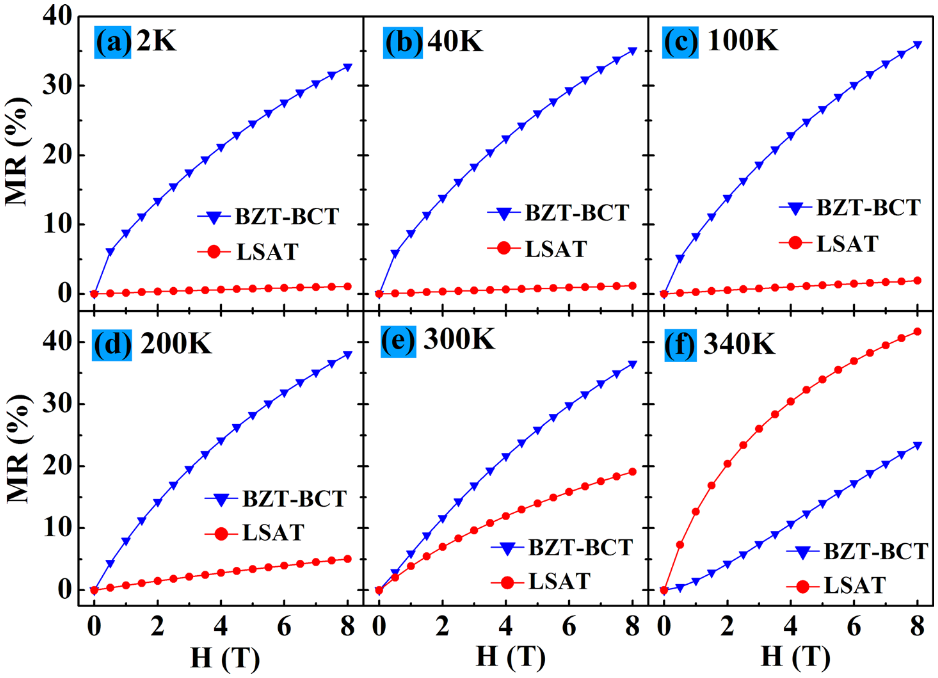

FIG. 5. Magnetic field dependence of the magnetoresistance of the LSMO films (∼16 nm) grown on BZT-BCT and LSAT substrates, as measured at different fixed temperatures.

are much larger than those of the LSMO epitaxial film. The MR value at $T = 2$ K and $H = 8$ T reaches ∼38%, approximately two orders of magnitude larger than that of the epitaxial one at the same temperature ($T = 2$ K) and magnetic field ($H = 8$ T), demonstrating dramatically enhanced MR effects in the LSMO polycrystalline film. We further measured the magnetic field dependence of the MR for the LSMO polycrystalline and epitaxial films at several fixed temperatures and showed the results in Figs. 5(a)–5(f). For $T \leq 200$ K, the MR values of the LSMO polycrystalline film are indeed much larger than those of the epitaxial film, consistent with the temperature dependence of MR shown in Figs. 4(b) and 4(d).

It is noted that the MR values of the polycrystalline film at $H = 2$, 4, 6, and 8 T are almost temperature independent from 2 K to T_C (∼275 K), with a rangeability of 3.6%–11% [Fig. 4(b)]. Namely, the MR of the polycrystalline film is insensitive to temperature for $T < T_C$, which is in stark contrast to the highly temperature-sensitive MR behaviors of the LSMO epitaxial film [Fig. 4(d)]. Further, the resistivity of the LSMO polycrystalline film shows pronounced upturn with decreasing temperature from $T \sim 38$ K, which is absent in the LSMO epitaxial film [Fig. 4(c)]. All these electronic transport and magnetoresistance behaviors are very likely linked to the polycrystalline nature of the LSMO film on BZT-BCT. Because of the existence of a large number of grain boundaries in the LSMO polycrystalline film, both the spin-polarized tunneling of charge carriers across grain boundaries and the scattering of charge carriers by disordered spins near grain boundaries would contribute significantly to the enhanced magnetoresistance for $T < T_C$.[30–32] For $T \geq 300$ K, the ferromagnetic spin ordering of the LSMO polycrystalline film almost disappears (Fig. 2). Consequently, the spin-polarized tunneling effect would be greatly suppressed at $T = 300$ K. Under such circumstance, the MR effect at $T \geq 300$ K is mainly contributed from the intrinsic magnetoresistance effect of the LSMO.

IV. CONCLUSIONS

We have fabricated LSMO/BZT-BCT lead-free multiferroic structures by depositing LSMO polycrystalline films on piezoelectrically active BZT-BCT ceramics substrates. Upon application of bipolar electric fields E to the BZT-BCT at room temperature, the variation of the resistivity of LSMO films with E displays butterfly-like behaviors which resemble the butterfly-like in-plane strain *versus* E curve for the BZT-BCT substrate, demonstrating nontrivial role of the piezoelectric strain in establishing the resistivity behaviors. With decreasing temperature, $\Delta\rho/\rho$ *versus* E curve becomes asymmetric gradually, which is attributed to non-180° domain rotation due to the freezing of ferroelectric domains at low temperatures. Further, MR of LSMO polycrystalline films at low temperatures are much larger than those of LSMO epitaxial films and are almost temperature independent from 2 K to T_C of the LSMO polycrystalline film, which is interpreted in terms of the contribution from the spin-polarized tunneling of charge carriers across grain boundaries.

SUPPLEMENTARY MATERIAL

See supplementary material for schematic experimental setups, magnetization versus temperature for the LSMO (32, 64, 128 nm), Electric-field-induced relative resistivity changes versus electric field and temperature for the LSMO (8, 16, 32, 64 nm)/BZT-BCT structures, Electric-field-induced in-plane strain for a BZT-BCT substrate, dielectric constants for a BZT-BCT substrate, and x-ray diffraction pattern for the LSMO/LSAT structure.

ACKNOWLEDGMENTS

This work was supported by the National Natural Science Foundation of China (Grant Nos. 51572278, 51502129, and 11574214).

[1] J. M. Hu, L. Q. Chen, and C. W. Nan, Adv. Mater. **28**, 15 (2016).
[2] R. C. Peng, J. M. Hu, K. Momeni, J. J. Wang, L. Q. Chen, and C. W. Nan, Sci. Rep. **6**, 27561 (2016).
[3] C. A. F. Vaz, F. J. Walker, C. H. Ahn, and S. Ismail-Beigi, J. Phys.: Condens. Matter **27**, 123001 (2015).
[4] R. K. Zheng, Y. Wang, H. L. W. Chan, C. L. Choy, and H. S. Luo, Phys. Rev. B **75**, 212102 (2007).
[5] W. P. Zhou, Y. Q. Xiong, Z. M. Zhang, D. H. Wang, W. S. Tan, Q. Q. Cao, Z. H. Qian, and Y. W. Du, ACS Appl. Mater. Interfaces **8**, 5424 (2016).
[6] T. Jiang, S. W. Yang, Y. K. Liu, Y. W. Yin, S. N. Dong, W. B. Zhao, and X. G. Li, Appl. Phys. Lett. **103**, 053504 (2013).
[7] Y. J. Zhang, M. Liu, L. Zhang, Z. Y. Zhou, B. Peng, C. Y. Wang, Q. J. Lin, Z.-D. Jiang, W. Ren, and Z.-G. Ye, Appl. Phys. Lett. **110**, 082902 (2017).
[8] Z. G. Wang, Y. J. Wang, H. S. Luo, J. F. Li, and D. Viehland, Phys. Rev. B **90**, 134103 (2014).
[9] Y. Lee, Z. Q. Liu, J. T. Heron, J. D. Clarkson, J. Hong, C. Ko, M. D. Biegalski, U. Aschauer, S. L. Hsu, M. E. Nowakowski, J. Wu, H. M. Christen, S. Salahuddin, J. B. Bokor, N. A. Spaldin, D. G. Schlom, and R. Ramesh, Nat. Commun. **6**, 5959 (2015).
[10] P. S. Li, Y. G. Zhao, S. Zhang, A. T. Chen, D. L. Li, J. Ma, Y. Liu, D. T. Pierce, J. Unguris, H. G. Piao, H. Y. Zhang, M. H. Zhu, X. Z. Zhang, X. F. Han, M. C. Pan, and C. W. Nan, ACS Appl. Mater. Interfaces **9**, 2642 (2017).
[11] M. Liu, O. Obi, J. Lou, Y. J. Chen, Z. H. Cai, S. Stoute, M. Espanol, M. Lew, X. D. Situ, K. S. Ziemer, V. G. Harris, and N. X. Sun, Adv. Funct. Mater. **19**, 1826 (2009).
[12] J. Wang, J. Ma, Z. Li, Y. Shen, Y. H. Lin, and C. W. Nan, J. Appl. Phys. **110**, 043919 (2011).
[13] J. W. Wang, Y. G. Zhao, C. Fan, X. F. Sun, S. Rizwan, S. Zhang, P. S. Li, Z. Lin, Y. J. Yang, W. S. Yan, Z. L. Luo, L. K. Zou, H. L. Liu, Q. P. Chen, X. Zhang, M. H. Zhu, H. Y. Zhang, J. W. Cai, X. F. Han, Z. H. Cheng, C. Gao, D. Xie, and T. L. Ren, Appl. Phys. Lett. **102**, 102906 (2013).
[14] R. V. Chopdekar and Y. Suzuki, Appl. Phys. Lett. **89**, 182506 (2006).
[15] W. Eerenstein, M. Wiora, J. L. Prieto, J. F. Scott, and N. D. Mathur, Nat. Mater. **6**, 348 (2007).
[16] H. F. Tian, T. L. Qu, L. B. Luo, J. J. Yang, S. M. Guo, H. Y. Zhang, Y. G. Zhao, and J. Q. Li, Appl. Phys. Lett. **92**, 063507 (2008).
[17] F. D. Czeschka, S. Geprägs, M. Opel, S. T. B. Goennenwein, and R. Gross, Appl. Phys. Lett. **95**, 062508 (2009).
[18] Z. X. Cheng, X. L. Wang, S. X. Dou, M. Osada, and H. Kimura, Appl. Phys. Lett. **99**, 092103 (2011).
[19] R. O. Cherifi, V. Ivanovskaya, L. C. Phillips, A. Zobelli, I. C. Infante, E. Jacquet, V. Garcia, S. Fusil, P. R. Briddon, N. Guiblin, A. Mougin, A. A. Uenal, F. Kronast, S. Valencia, B. Dkhil, A. Barthelemy, and M. Bibes, Nat. Mater. **13**, 345 (2014).
[20] A. Alberca, N. M. Nemes, F. J. Mompean, N. Biskup, A. de Andres, C. Munuera, J. Tornos, C. Leon, A. Hernando, P. Ferrer, G. R. Castro, J. Santamaria, and M. Garcia-Hernandez, Phys. Rev. B **84**, 134402 (2011).
[21] W. F. Liu and X. B. Ren, Phys. Rev. Lett. **103**, 257602 (2009).
[22] R. K. Zheng, Y. Wang, J. Wang, K. S. Wong, H. L. W. Chan, C. L. Choy, and H. S. Luo, Phys. Rev. B **74**, 094427 (2006).
[23] L. Zhang, X. B. Ren, and M. A. Carpenter, Phys. Rev. B **95**, 054116 (2017).
[24] M. Zheng, M. M. Yang, Q. X. Zhu, X. Y. Li, G. Y. Gao, R. K. Zheng, Y. Wang, X. M. Li, X. Shi, H. S. Luo, and X. G. Li, Phys. Rev. B **90**, 224420 (2014).
[25] J. Klein, C. Höfener, S. Uhlenbruck, L. Alff, B. Büchner, and R. Gross, Europhys. Lett. **47**, 371 (1999).
[26] J. Yang, B. C. Zhao, R. L. Zhang, Y. Q. Ma, Z. G. Sheng, W. H. Song, and Y. P. Sun, Solid State Commun. **132**, 83 (2004).
[27] K. H. Kim, J. Y. Gu, H. S. Choi, D. J. Eom, J. H. Jung, and T. W. Noh, Phys. Rev. B **55**, 4023 (1997).
[28] A. J. Millis, Nature **392**, 147 (1998).
[29] M. Fath, S. Freisem, A. A. Menovsky, Y. Tomioka, J. Aarts, and J. A. Mydosh, Science **285**, 1540 (1999).
[30] H. Y. Hwang, S.-W. Cheong, N. P. Ong, and B. Batlogg, Phys. Rev. Lett. **77**, 2041 (1996).
[31] M. Patra, A. Roy, S. Majumdar, and S. Giri, Appl. Phys. Lett. **94**, 212107 (2009).
[32] X. W. Li, A. Gupta, G. Xiao, and G. Q. Gong, Appl. Phys. Lett. **71**, 1124 (1997).